CO_2 Sink Capacity of the Western Arctic Ocean in Early Winter: November 2018

A. Murata[1], J. Inoue[2], S. Nishino[3], and S. Yasunaka[1]

[1]Global Ocean Observation Research Center, Japan Agency for Marine-Earth Science and Technology, 2-15, Natsushima, Yokosuka, Kanagawa, 237-0061, Japan, [2]Meteorology and Glaciology Group, National Institute of Polar Research, 10-3, Midori-cho, Tachikawa, Tokyo 190-8518, Japan, [3]Institute of Arctic Climate and Environment Research, Japan Agency for Marine-Earth Science and Technology, 2-15, Natsushima, Yokosuka, Kanagawa, 237-0061, Japan

Correspondence to:

Akihiko Murata,

murataa@jamstec.go.jp

Key Points:

- In Nov 2018, shelf waters in the western Arctic Ocean acted as a sink for atmospheric CO_2 as large as in summer, late Aug−Sep 2017
- In the marginal ice zone, cooling of Pacific-origin water was the main cause of a surface seawater pCO_2 drawdown of 70−90 atm
- Total alkalinity controlled spatial distributions of surface seawater pCO_2 via conservative changes of total dissolved inorganic carbon

Abstract To investigate CO_2 sink capacity in the western Arctic Ocean (north of 65°N), we conducted underway, ship-based observations of partial pressures of CO_2 (pCO_2) and total dissolved inorganic carbon (TCO_2) in surface seawater in early winter (November 2018). From these two properties of the seawater inorganic carbon system, we calculated total alkalinity (TA). In the early winter, surface seawater pCO_2 in most places was lower than atmospheric pCO_2. The weighted mean of the air-sea fluxes of CO_2 were calculated to be -7.5 ± 1.6 mmol m^{-2} d^{-1}. The calculated fluxes implied that the area acted as a moderate sink for atmospheric CO_2 in early winter, and its rate of CO_2 uptake was comparable to that (-8.0 ± 1.7 mmol m^{-2} d^{-1}) in summer (late August−September 2017). Spatial variations of surface seawater pCO_2 in the early winter could be attributed mostly to conservative changes of TCO_2 and TA, which together accounted for more than 70% of the pCO_2 variations. In the marginal ice zone, however, there was a drawdown of surface seawater pCO_2 by 70−90 atm due to horizontal advection of water with an anomalously high temperature from the Pacific Ocean and its subsequent cooling. We found that TA was an important determinant of the spatial variations of pCO_2 in the western Arctic Ocean because of the conservative nature of the changes of TA and TCO_2 during mixing of water masses. This conservative behavior was observed in both the early winter and summer.

Plain Language Summary The characteristics of the Arctic Ocean are changing because of a reduction of sea ice caused by global warming. Carbon cycling may also change considerably in response to global warming and associated environmental changes. To evaluate how much CO_2 is currently taken up by the ocean, we conducted ship-based observations of atmospheric and surface seawater partial pressures of CO_2 (pCO_2) and related seawater properties on the Pacific Ocean side of the Arctic Ocean (north of 65°N) in early winter, when few such observations have been conducted because of the seasonal expansion of sea ice. In early winter (November 2018), surface seawater pCO_2 was lower than atmospheric pCO_2, except in the southern parts of the study area. This result implies that the area acted as a sink for atmospheric CO_2. In early winter, when rates of biological processes associated with phytoplankton activities were low because there was little sunlight, spatial variations of surface seawater pCO_2 could be explained mostly by water mixing, except in the area close to sea ice, where the low water temperature decreased the pCO_2. We highlight the role of total alkalinity, which is one of the properties of the oceanic carbonate system, as a determinant of the potential of the ocean to act as a sink for CO_2.

1 Introduction

The ocean is estimated to have absorbed about 2.5 ± 0.6 GtC yr^{-1} (about 24%) of the anthropogenic CO_2 that has been released into the atmosphere by human activities such as burning of fossil fuels, deforestation, and cement production (Friedlingstein et al., 2020). Thus, the ocean plays a major role in alleviating global warming by its uptake of anthropogenic CO_2. However, the capacity of the ocean to absorb anthropogenic CO_2 is unlikely to remain unchanged in the future. Ongoing global warming and the associated changes of climate are expected to change ocean physical and biogeochemical conditions that control air-sea CO_2 exchanges. Periodic assessment of spatiotemporal changes of oceanic CO_2 is therefore crucial.

Estimation of air-sea fluxes of CO_2 based on observations of partial pressures of atmospheric and surface seawater CO_2 (pCO_2) is a straightforward approach to the evaluation of the CO_2 sink capacity of the ocean. In fact, Takahashi et al. (2002) have used this approach to estimate the CO_2 sink of the global ocean; they compiled about 960,000 surface seawater pCO_2 data, and estimated the annual uptake of CO_2 by the global ocean to be 2.2 (−19% to +22%) PgC yr^{-1}. In a later study, wherein the number of pCO_2 data was increased to 3 million, Takahashi et al. (2009) estimated the total ocean CO_2 uptake, including anthropogenic CO_2, to be 2.0 ± 1.0 PgC yr^{-1}. In 2007, following these pioneering studies, the international marine carbon community decided to produce a database of surface seawater pCO_2 (IOCCP, 2007). After quality-control of the data by the community using an agreed procedure, the database was made available in 2011 (Pfeil et al., 2013; Sabine et al., 2013); since then, revised versions with increased numbers of data have been published (Bakker et al., 2014; 2016). Use of these datasets has made it possible to discuss not only the annual mean and seasonal variations of surface seawater pCO_2 but also their interan-

nual variations and long-term trends (Rödenbeck et al., 2013; Landschützer et al., 2014; Iida et al., 2015). In these global-scale surveys, however, estimates for the Arctic Ocean have not been included at all, or only partial estimates have been included. The reason for this omission is that measurements of surface seawater pCO_2 have been sparse in the Arctic Ocean, because it is hard to conduct ship-based observations in an ocean with sea ice, and because the presence of sea ice has been thought to block air-sea exchanges of CO_2. The Arctic Ocean has therefore been regarded as not significant with respect to global-scale estimates of air-sea CO_2 fluxes. This situation has recently been changing, however, because global warming has reduced the area of the Arctic Ocean covered by sea ice and thereby made it easier for CO_2 to be taken up by the Arctic Ocean in the summer. Extensive areas of open sea presumably facilitate air-sea exchanges of CO_2.

The Arctic Ocean is generally considered to act as a sink for atmospheric CO_2 because the solubility of CO_2 is negatively correlated with water temperature, and the long photoperiods during the summer stimulate photosynthetic uptake of CO_2 that reduces CO_2 concentrations at the sea surface (Bates et al., 2006). Nevertheless, the question of whether the Arctic Ocean acts as a significant sink or source of atmospheric CO_2 is still being debated because observations in the Arctic Ocean have been limited geographically and seasonally (Yasunaka et al., 2016). Measurements of surface seawater pCO_2 have previously been made in some subregions of the Arctic Ocean during the ice-free season. Murata and Takizawa (2003), who have conducted underway pCO_2 observations in the shelf and slope waters of the western Arctic Ocean (WAO) in summer, have found that high-latitude continental margins become a moderate to strong CO_2 sink in that season. Nakaoka et al. (2006) have estimated surface seawater pCO_2 in the Greenland Sea and Barents Sea based on discrete sampling of air equilibrated with seawater and have discovered that those seas absorb atmospheric CO_2 throughout the year. Omar et al. (2007) have established an empirical relationship between the surface seawater fugacity of CO_2 (fCO_2, practically almost equal to pCO_2) and phosphate concentrations, water temperature, and salinity in the Atlantic sector of the Barents Sea. They used the relationship to analyze timeseries data and showed that the region was an annual sink of atmospheric CO_2. Gao et al. (2012), who measured surface seawater pCO_2 along the 169°W transect of the WAO in summer, showed that the shelf and slope waters are a sink for atmospheric CO_2 in general and that the surface waters of the central basin are a moderate CO_2 sink. To reduce the large uncertainty of estimated air-sea fluxes of CO_2 in the Barents Sea, Lauvset et al. (2013) have mapped the distributions of surface seawater fCO_2 in the Barents Sea with the aid of satellite data and model outputs. Their results have confirmed that the Arctic Ocean is as strong a CO_2 sink as estimated previously. Evans et al. (2015) have calculated sea-air CO_2 exchange in the western Arctic coastal ocean using directly measured and calculated pCO_2. They assessed the CO_2 exchange under existing or reduced sea-ice conditions and have concluded that carbon uptake in the region would be increased in the future under reduced sea-ice con-

ditions. Burgers et al. (2017), who conducted underway pCO_2 observations in the Eastern Canadian Arctic in summer, reported that surface seawater pCO_2, though highly variable spatially, never exceeded atmospheric CO_2. These studies collectively show that the Arctic Ocean acts as a sink for atmospheric CO_2, although each study dealt with only a subregion of the Arctic Ocean. Using a self-organizing map technique, Yasunaka et al. (2016) have estimated annual uptake of CO_2 by the entire Arctic Ocean (65°N) to be 180 $TgCyr^{-1}$ with an uncertainty of 210 $TgCyr^{-1}$. The large uncertainty resulted from the sparseness of pCO_2 measurements, and an improved estimate successfully reduced the uncertainty to 130 $TgCyr^{-1}$ (Yasunaka et al., 2018).

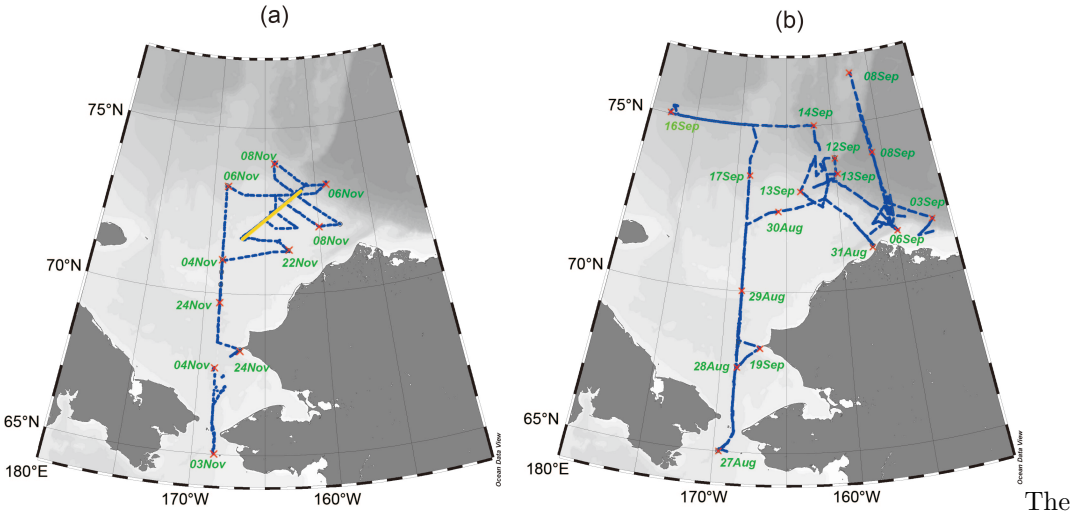

The goal of the present study was to clarify the capacity of the WAO to take up CO_2 in early winter, when pCO_2 measurements have rarely been conducted because of seasonal expansion of sea ice. To evaluate this capacity quantitatively, we calculated air-sea CO_2 fluxes. To account for the observed spatial variations of surface seawater pCO_2, we examined the variations of surface seawater temperature (SST), surface seawater salinity (SSS), surface seawater total dissolved inorganic carbon (TCO_2), and surface seawater total alkalinity (TA) calculated from pCO_2 and TCO_2. While performing these calculations, we scrutinized spatial variability, especially in the marginal ice zone (MIZ), because the effects of physical and biogeochemical processes that can cause variations of marine carbonate system properties are complex. To clearly characterize the spatial variations in the seasonal expansion of sea ice, we compared the data obtained in summer 2017 with the data from early winter. We assessed the results obtained in the present study in the context of results from previous studies to characterize the capacity of the WAO to function as a CO_2 sink during the seasonal expansion of sea ice.

2 Shipboard Observations

Data used in the present study were collected during two cruises conducted by

the R/V *Mirai* of the Japan Agency for Marine-earth Science and Technology (JAMSTEC) in 2017 and 2018 as part of the Arctic Challenge for Sustainability (ArCS) project. During the 2018 cruise (ID: MR18-05C), the observations in the WAO (north of 65°N, Figure1a) were made during 3–25 November. The main purpose of the cruise was to understand air-ice-sea coupled physical processes in early winter and to use that understanding to improve the forecasting skills of numerical models (Inoue, 2021). During the cruise, we used underway measuring systems to measure not only physical properties such as water temperature, salinity, and current velocities but also carbonate system properties such as atmospheric and surface seawater pCO_2 and surface seawater TCO_2. In November, sea ice usually prevents research vessels from penetrating deeply into the Arctic Ocean. In 2018, however, the R/V *Mirai* was able to enter the Chukchi Sea north of 74°N, probably because expansion of sea ice was delayed by an inflow of warm water (> 5°C) that was observed south of the Bering Strait (Kodaira et al., 2020). We intensively surveyed spatial variations of the properties of seawater in the MIZ during daily repeat observations when the research vessel approached closest to sea ice (Figure 1a). For details of the observations, please refer to Kodaira et al. (2020) and Inoue et al. (2021). In the present study, we defined the MIZ as the area where the repeat observations were made (yellow line in Figure 1a).

During the 2017 cruise (ID: MR17-05C), observations were made during the summer, from 27 August to 21 September. Because the sea ice reached its seasonal minimum for the year during that time, we could conduct meteorological and hydrographic observations over a wider area, including the area along the western edge of the Canada Basin (Figure 1b), than in 2018. We measured the pCO_2 and TCO_2 continuously in the same way that we did in 2017.

3. Analytical Procedures

3.1. Underway pCO_2

Continuous measurements of atmospheric and surface seawater pCO_2 were made with the CO_2-measuring system (Nihon ANS, Inc.) installed on the R/V *Mirai*. The system comprised two kinds of detectors: a non-dispersive infrared gas analyzer (NDIR, Li-COR LI-7000, modified by Nihon ANS, Inc.) and an off-axis, integrated-cavity, output spectroscopy gas analyzer (Off-Axis ICOS; 911-0011, Los Gatos Research). The system also included an air-circulation module and a shower-head type equilibrator. To measure the concentration (mole fraction) of CO_2 in dry air (xCO_2a), air sampled from the bow of the ship (~13 m above sea level) was introduced into the NDIR and the Off-Axis ICOS through a dehydrating route. To measure in surface seawater the concentrations of CO_2 in dry air (xCO_2s), air equilibrated with seawater within the equilibrator was introduced into the NDIR and the Off-Axis ICOS through the same dehydration flow route used for xCO_2a. The flow rate of the equilibrated air was 600–800 ml min^{-1}. The seawater was sampled by a pump placed ~4.5 m below the sea surface. The flow rate of seawater in the equilibrator was 4000–5000 ml min^{-1}. The CO_2-measuring system was set to repeat the measurement cycle that in-

cluded four kinds of CO_2 standard gases (219, 328, 389, and 418 ppmv), the concentrations of which were traceable to the WMO2007 scale, xCO_2a (twice), and xCO_2s (7 times). The xCO_2 values were converted to pCO_2 at 100% relative humidity with SST and SSS. For the MR18-05C cruise, the pCO_2 data (n = 3237) measured by the Off-Axis ICOS were used, whereas for the MR17-05C cruise (Figure 1b), the pCO_2 data ($n = 4354$) measured by the NDIR were used, because the MR17-05C cruise was a test cruise for the Off-Axis ICOS detector.

Averages of xCO_2a in the WAO were calculated to be 411.5 ± 1.0 ppmv and 396.3 ± 1.0 ppmv for the MR18-05C and MR17-05C cruises, respectively, and were comparable to the monthly CO_2 concentrations of 412.18 ppmv and 397.59 ppmv observed at Point Barrow, Alaska (71°19' N, 156°36' W).

The repeatability of the xCO_2 measurements was estimated based on repeated measurements of the concentrations of standard gases to be <0.1 ppmv and <0.2 ppmv during the MR18-05C and MR17-05C cruises, respectively.

3.2. Underway TCO_2

Continuous measurements of surface seawater TCO_2 were made with a TCO_2-measuring system (Nihon ANS, Inc.) installed on the R/V *Mirai*. The system used a coulometer (Nihon ANS, Inc.) as a detector. The system's underway water-sampling unit automatically collected surface seawater in a ~300-ml borosilicate glass bottle after overflowing the bottle with three times its volume. Before measurements, water samples were kept at 20°C. The seawater was then transferred into a pipette (~15 ml), which was maintained at 20°C by a water jacket through which water was circulated from a water bath set at 20°C. The CO_2 dissolved in the seawater sample was extracted in a stripping chamber of the CO_2 extraction system by adding about 2 ml of phosphoric acid (~10 % v/v). The stripping chamber was ~25 cm long and had a fine frit at the bottom. The acid was added to the stripping chamber from the bottom of the chamber by pressurizing an acid bottle for a fixed time to push out the right amount of acid. The bottle was pressurized with nitrogen gas (99.9999%). After the acid was transferred to the stripping chamber, a seawater sample maintained in a pipette was introduced into the stripping chamber by the same method used to add acid. After reacting with the phosphoric acid, the seawater was stripped of CO_2 by bubbling with nitrogen gas through the fine frit at the bottom of the stripping chamber. The CO_2 stripped in the chamber was carried by the nitrogen gas (flow rate of 140 ml min^{-1}) to the coulometer through a dehydrating module. The TCO_2-measuring system was calibrated with certified reference materials (CRMs: batches 166 and 149 for MR18-05C and MR17-05C, respectively) provided by Prof. A. G. Dickson of Scripps Institution of Oceanography. We obtained 872 and 1151 data for MR18-05C and MR17-05C, respectively.

The repeatability of the TCO_2 measurements was estimated based on measurements of CRMs to be < 2 mol kg^{-1} for both cruises.

3.3. Calculation of TA

Surface seawater TA was calculated from surface seawater pCO_2 and surface seawater TCO_2, both of which were measured continuously during the cruises (sections 3.1 and 3.2). However, because the sampling frequencies were different for TCO_2 and pCO_2, a compromise had to be made for calculation purposes. Because the pCO_2 data were obtained more frequently than the TCO_2 data, we used pCO_2 data that were collected as close as possible in time to the times when the TCO_2 measurements were made. For this purpose, we chose pCO_2 data that were measured within 2.5 minutes before or after the TCO_2 measurements. The TA was then computed from TCO_2, pCO_2, SST, and SSS. There were two sets of SST and SSS data, one set for TCO_2 and the other set for pCO_2. We averaged the SST and SSS values to calculate the TA.

Values of TA were calculated using the Microsoft Excel/VBA version of co2sys.xls by G. Pelletier, E. Lewis and D. Wallace, which is a modified spreadsheet excerpted from CO2SYS.EXE by Lewis and Wallace (1998). For the calculation, we used the equilibrium constants of Lueker et al. (2000), which were refit from Mehrbach et al. (1973), and nutrients were assumed to be depleted. Total boron was estimated based on Uppstrom (1974).

The number of calculated TA values on each cruise equaled the number of TCO_2 values. The uncertainty of the calculated TA was estimated to be -0.1 ± 5.8 mol kg^{-1} (Woosley et al., 2017).

3.4. Air-sea Fluxes of CO_2

The air-sea flux, F (mmol m^{-2} d^{-1}) of CO_2 was computed using the following equation:

$$F = k \times s \times pCO_2 \quad (1)$$

where k (cm h^{-1}) indicates the transfer velocity, and s is the solubility (mmol m^{-3} atm^{-1}) of CO_2 (Weiss, 1974). The value of k was calculated based on Wanninkhof (2014):

$$k = 0.251 \times U^2 \times \left(\frac{Sc}{660}\right)^{-0.5} \quad (2)$$

where U (m s^{-1}) is the wind speed at 10 m in height. The parameter Sc is the Schmidt number determined as a function of water temperature (Wanninkhof, 2014).

The pCO_2 was calculated by subtracting the surface seawater pCO_2 from atmospheric pCO_2, which was the average of the observed pCO_2 in the WAO. For the calculation of U in Eq. (2), the wind speeds observed on board the R/V *Mirai* were first corrected to those at a height of 10 m above the sea surface (Large & Pond, 1981). The averages of the corrected wind speeds in the WAO were then used for U.

We calculated air-sea fluxes of CO_2 on the assumption of ice-free conditions, even if the observations were made close to sea ice.

4. Results

4.1. Distributions of Surface Seawater pCO_2, SST, and SSS

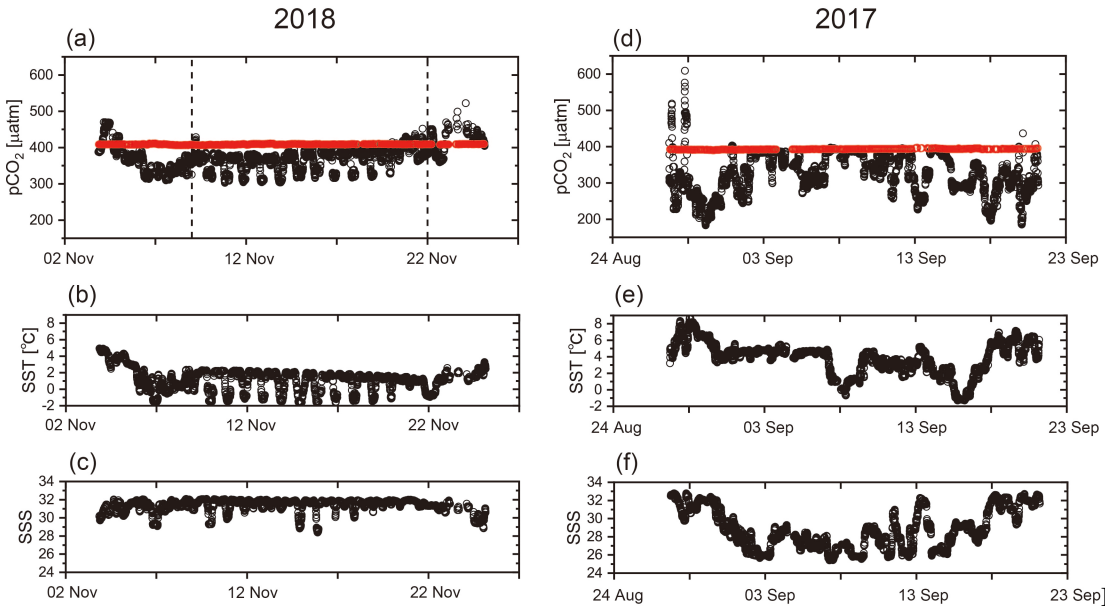

Distributions of surface seawater pCO_2 in the early winter are shown in Figure 2a versus the day of sampling, along with those of SST (Figure 2b) and SSS (Figure 2c). Surface seawater pCO_2 was usually lower than atmospheric pCO_2 (= 408.9 ± 1.0 atm, red circles in Figure 2a), except for the pCO_2 values observed during the early and late part of the observation period and those observed on the first day of the repeat observations (9 November). Surface seawater pCO_2 values higher than atmospheric pCO_2 values were observed in shelf waters (Figure S1a). The maximum surface seawater pCO_2 (523 atm) was found at 167.3°W, 68.2°N. The most distinct characteristic of the pCO_2 distribution was that it varied in an up-and-down manner in the MIZ; surface seawater pCO_2 decreased abruptly from high values of 370−400 atm to low values of 300−310 atm. The shipboard observations in the MIZ were conducted by cruising back and forth in a relatively small area covering longitudes of 180°−150°W and latitudes of 65°N−77°N (Figure 1a). During the observations, the underway pCO_2 measurements were made along a repeat line set in a southwest-northeast direction (Figure 1a). The up-and down variations implied abrupt spatial changes of pCO_2 by 70−90 atm over a distance of ~130 km. The minimum pCO_2 of 303 atm was found at 161.7°W, 73.1°N in the MIZ. The results (Figure 2a, d) indicated that the area generally acted as a sink for atmospheric CO_2 in the early winter.

Both SST (Figure 2b) and SSS (Figure 2c) generally varied in parallel with surface seawater pCO_2, especially in the MIZ, where the up-and-down variations correlated positively with the pCO_2. In the MIZ, the SST changed from ~2.0°C to −2.0°C. The latter temperature is close to the freezing point of seawater

and reflects the fact that the observations were made near sea ice. SSTs higher than 2.0°C were found outside the MIZ. In particular, SSTs of 4.0−5.0°C were observed during the early part of the observation period and were found south of 70°N (Figure S1b). The variations of SSS were not correlated distinctly with the associated variations of pCO_2.

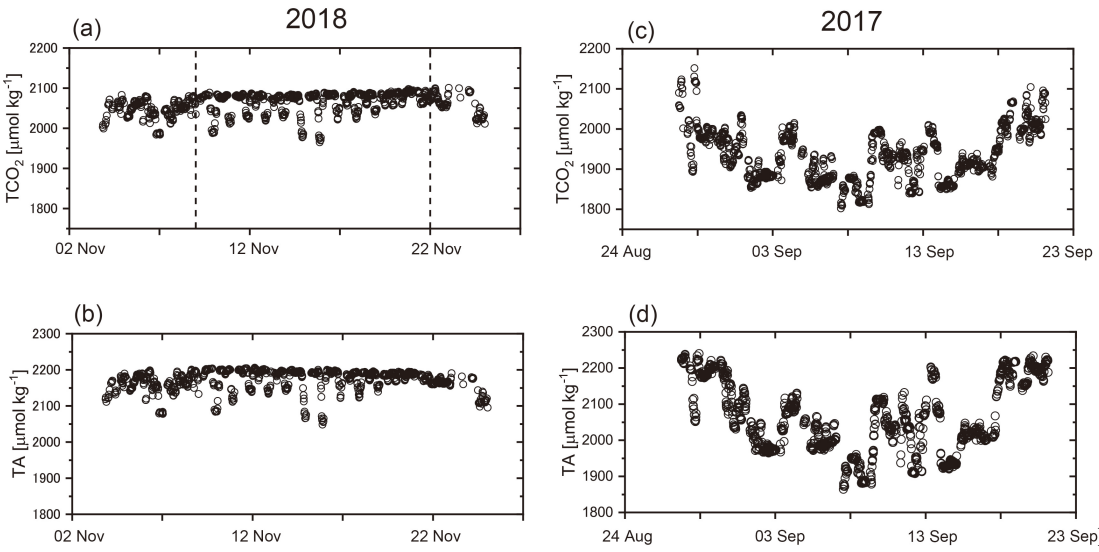

Figures 2d, 2e, and 2f show surface seawater pCO_2, SST, and SSS, respectively, versus time in the summer. Seasonal effects caused atmospheric pCO_2 to be lower in summer (= 393.2 ± 1.1 atm) than in early winter (Figure 2a). The fact that surface seawater pCO_2 was generally lower than atmospheric pCO_2, except during the early part of the observation period, suggests that the area as a whole acted as a sink for atmospheric CO_2. The pCO_2 maximum (609 atm) and minimum (183 atm) were found at 168.8°W, 68.0°N and at 168.7°W, 71.8°N, respectively (Figure S1d). The pCO_2 distributions were not as positively correlated with SST (Figure 2e) and SSS (Figure 2f) in the summer as they were in the early winter (Figures 2a, b, and c).

One of the most distinctive differences between the pCO_2 distributions in early winter and summer was the range of the distributions. The ranges of pCO_2 in the early winter and the summer were 220 atm and 426 atm, respectively. The ranges of both SST and SSS were also smaller in early winter versus summer: 6.5 °C and 10.0 °C, respectively, for SST, and 3.7 and 7.4, respectively, for SSS. This difference between early winter and summer is discussed in detail and compared with the results of previous studies in section 6.1.

4.2. Distributions of TCO_2 and TA

Figure 3a shows the values of surface seawater TCO_2 in the early winter versus time. The upper limit of TCO_2 was nearly constant at ~2090 mol kg^{-1} throughout the observation period. The variations of TCO_2 were coherent with those of

the surface seawater pCO_2 (Figure 2a), especially in the MIZ. Figure 3b shows the distributions of surface seawater TA in early winter. The upper bound of the TA was also nearly constant at ~2190 mol kg^{-1}, and the variations were coherent with those of the surface seawater pCO_2.

Figure 3c shows the time series of surface seawater TCO_2 in the summer. The overall pattern of the TCO_2 time series was concave up with some short-term up-and-down variations. The highest values (>2050 mol kg^{-1}) occurred near the start and end of the time series and corresponded to observations made in shelf waters south of 68°N (Figure S2c). TCO_2 was clearly higher and lower in the southern and northern parts of the study area, respectively (Figure S2c). The variations of TCO_2 were not as coherent with those of pCO_2 (Figure 2d) as they were in the early winter, but TCO_2 correlated positively with SSS (Figure 2f). The characteristics of the TA time series in the summer were similar to those of the TCO_2 time series, i.e., a concave up pattern with short-term up-and-down variations. The geographical distribution of TA in the summer was similar to that of TCO_2: high in the south and low in the north (Figure S2d). The variations of TA were not coherent with those of pCO_2, but TA values were positively correlated with SSS.

One of the most conspicuous differences in the distributions of TCO_2 and TA between the early winter and summer was the range of each property. In the early winter, the ranges of TCO_2 and TA were much smaller, 136 mol kg^{-1} and 157 mol kg^{-1}, respectively, than in the summer, 349 mol kg^{-1} and 375 mol kg^{-1}, respectively.

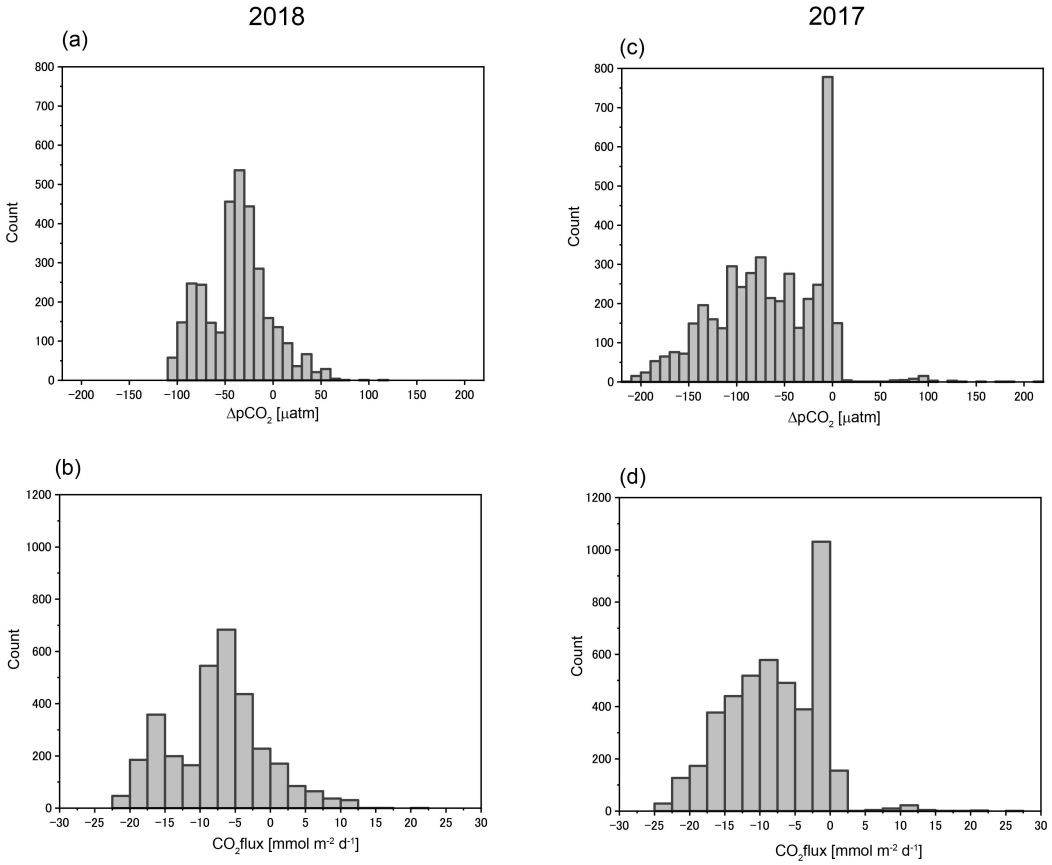

4.3. Distributions of pCO_2 and Air-sea Fluxes of CO_2

To evaluate the CO_2 sink capacity of the WAO in early winter, we created histograms of the pCO_2 and calculated CO_2 fluxes (Figure 4). In the early winter, there were two peaks of pCO_2 (Figure 4a): a higher peak at -40 to -30 atm ($n = 536$) and a lower peak at -90 to -70 atm ($n = 491$). The latter peak was observed mainly in slope waters (Figure S3a). The pCO_2 values varied from -105 atm to 105 atm. In the summer, there was an extremely large peak at -10 to 0 atm (Figure 4c, $n = 778$) that was observed mostly in slope waters (Figure S3c). There was a smaller second peak at -80 to -70 atm ($n = 318$). The pCO_2 in the summer varied from -215 atm to $+215$ atm, a range (430 atm) that was twice as large as the corresponding range (210 atm) in the early winter.

The histogram of CO_2 fluxes in the early winter (Figure 4b) revealed a pattern consistent with that of pCO_2. There were two peaks in the histogram, one at -7.5 to -5.0 mmol m^{-2} d^{-1} ($n = 683$) and the other at -17.5 to -15.0 mmol m^{-2} d^{-1} ($n = 358$). In the summer (Figure 4d), the largest peak appeared at -2.5 to 0.0 mmol m^{-2} d^{-1} ($n = 1031$), and a smaller peak appeared at -10.0 to

-7.5 mmol m^{-2} d^{-1} ($n = 578$). This pattern was consistent with the pattern of pCO_2 (Figure 4c).

The weighted means and standard deviations of the CO_2 fluxes were calculated to be -7.5 ± 1.6 and -8.0 ± 1.7 mmol m^{-2} d^{-1} in the early winter and summer, respectively. These results indicate that the area acted as a moderate sink for atmospheric CO_2 in both the early winter and summer.

5. Decomposition of Changes of Surface Seawater pCO_2

To determine which properties most affected surface seawater pCO_2 in the WAO, we decomposed the changes of pCO_2 ($dpCO_2$) into partial changes of pCO_2 due to changes of SST ($dpCO_{2\_SST}$), TCO_2 ($dpCO_{2\_TCO2}$), TA ($dpCO_{2\_TA}$), and freshwater ($dpCO_{2\_fw}$) (Sarmiento and Gruber, 2006; Ouyan et al., 2020) as follows (see Text S1 for the details):

$$dpCO_2 = dpCO2\_SST + dpCO_{2\_TCO_2} + dpCO2\_TA + dpCO2\_fw \quad (3)$$

Starting from the first observations north of 65°N during each cruise, we computed individual terms on the right-hand side of Eq. 3 from the first and second observations, and we repeated the computation one by one up to the last observation on each cruise north of 65°N. In addition, we used selected data to calculate $dpCO_2$ in the MIZ so that we could assess the spatial variability of surface seawater pCO_2 close to the sea ice (section 5.2). The averages and standard deviations of the differences of the calculated (j+1)th pCO_2 (= (j)th observed pCO_2 + (j)th $dpCO_2$) from the observed (j+1)th pCO_2 were -0.3 ± 8.7 atm, -0.5 ± 15.8 atm, and -7.0 ± 25.6 atm for the early winter, summer, and the MIZ, respectively. This result implies that the pCO_2 variations could be adequately explained by the four partial changes of pCO_2.

To quantify the relative contribution of property i to $dpCO_2$, we calculated its contribution ratio (CR_i in %) as follows:

$$\mathbf{CR_i} = \frac{|\mathbf{dpCO_{2\_i}}|}{|\mathbf{dpCO_{2\_SST}}| + |dpC\mathbf{O_{2\_TCO_2}}| + |dpC\mathbf{O_{2\_TA}}| + |dpC\mathbf{O_{2\_fw}}|} \times \mathbf{100}, \quad (4)$$

where $dpCO_{2\_i}$ is the change of pCO_2 due to a change of property i, where i = SST, TCO_2, TA, or freshwater (fw).

5.1. Decomposed Changes of Surface Seawater pCO_2 in Each Season

Table 1 lists the averages and standard deviations of the CR_i in the early winter and in the summer. It is apparent from Table 1 that TCO_2 and TA had by far the largest effects on the spatial variations of surface seawater pCO_2 ($dpCO_2$), about 40% and 36%, respectively, of the total effects. Together these the two properties accounted for 76% of the spatial variations of the surface seawater pCO_2. The fact that the correlations between $dpCO_{2\_TCO2}$ and $dpCO_{2\_TA}$ were -0.77 and -0.68 in the early winter and summer, respectively, weakened the combined influences of $dpCO_{2\_TCO2}$ and $dpCO_{2\_TA}$ on the pCO_2 variations. The contributions of SST and freshwater were comparable to each other in both seasons.

Property (i)	CR_i %		
	Early winter	Summer	MIZ
SST	(14.3)	(17.4)	(8.5)
TCO_2	(18.1)	(16.0)	(9.4)
TA	(17.8)	(16.0)	(8.8)
Freshwater	(13.1)	(13.3)	(5.4)

5.2 Decomposed Changes of Surface Seawater pCO_2 in the MIZ

To decompose the changes of the pCO_2, we first arbitrarily selected peaks and troughs from the up-and-down variations of the pCO_2 (Figure 2a). We chose 12 peaks and 11 troughs from the pCO_2 time series, together with the corresponding SST, SSS, TCO_2, and TA (Table S1). Starting with the peak observed on 9 November, we computed individual terms on the right-hand side of Eq. 3 and calculated the difference between those terms for the peak on 9 November and the trough on 10 November. A similar comparison was made for successive pairs of peaks and troughs until we had computed the difference of the terms for the trough on 19 November and the peak on 20 November.

Figure 5 illustrates the contribution of each property to the changes of pCO_2 between pairs of peaks and troughs. It is readily apparent that $dpCO_{2\_SST}$ made the largest contribution. In many cases, $dpCO_{2\_TCO2}$ and $dpCO_{2\_TA}$ were nearly equal in magnitude to each other, but in 16 of 22 cases, their effects were opposite in sign. The $dpCO_{2\_fw}$ values were the smallest in magnitude, but their signs were in all cases the same as the signs of $dpCO_{2\_SST}$. The strong correlation between $dpCO_{2\_SST}$ and $dpCO_{2\_fw}$ ($r = 0.98$) suggests that they were functions of the same physical processes, such as dilution and cooling of seawater by sea ice in the MIZ.

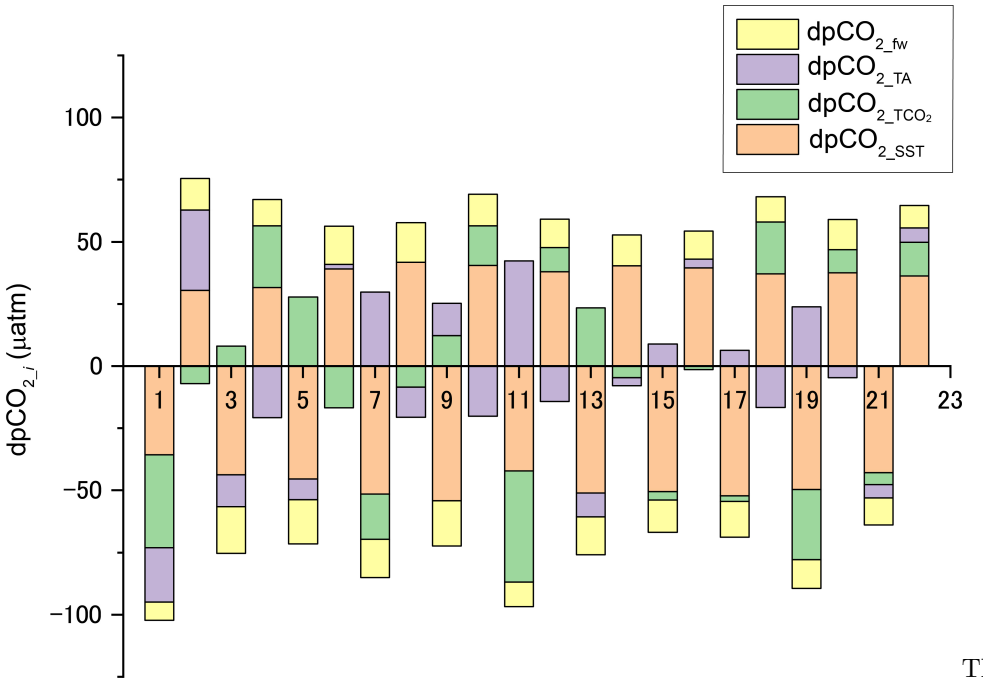

The $dpCO_{2\_TCO2}$ values were negatively correlated ($r = -0.55$) with $dpCO_{2\_TA}$, although the correlation coefficient was not as large in magnitude as the correlation coefficient in early winter.

The averages and standard deviations of the CR_i calculated for the MIZ (last column in Table 1) support the findings stated in the previous paragraph. Namely, variations of SST accounted for nearly 50% of the spatial variations of pCO_2 ($dpCO_2$). The next largest contribution came from TCO_2, but its contribution was approximately one-third the contribution of SST. In order of magnitude, the contributions of TA and freshwater were similar to that of TCO_2.

6. Discussion

6.1. Processes Controlling the Distributions of Surface Seawater pCO_2

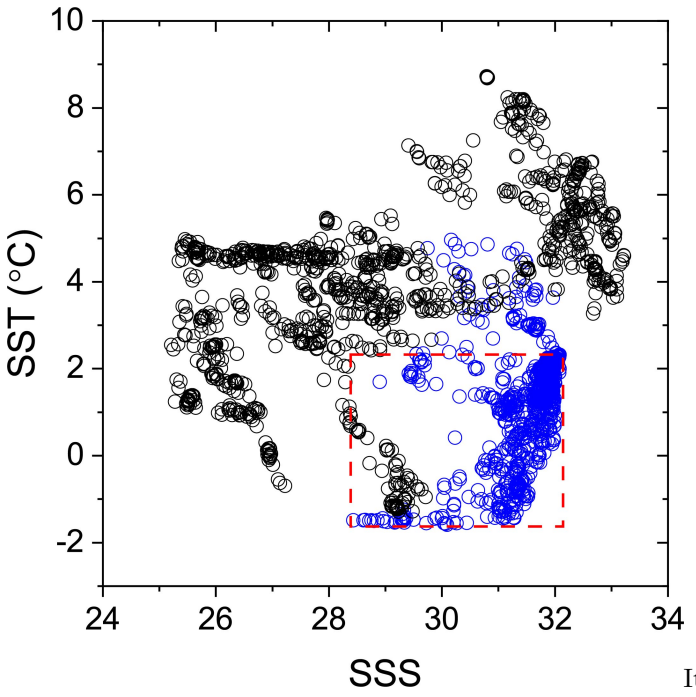

It has been reported that oceanic CO_2 in the WAO displays high temporal and spatial variations (Murata & Takizawa, 2003; Gao et al., 2012). One of the reasons for these variations is that several different water masses enter the WAO from the Pacific Ocean through the Bering Strait and are mixed with local waters. The inflowing waters are classified as Bering Shelf Water, Alaskan Coastal Water, and Anadyr Water (Coachman et al., 1975; Cai et al., 2014; Gong & Pickart, 2015). These water masses are modified in shelf and slope regions of the ocean by physical and biogeochemical processes. In addition to these water masses from the Pacific Ocean, freshwater from rivers and melting of sea ice are also involved in water mixing. The T−S diagram (Figure 6) supports the conclusion that several different water masses are involved in the mixing, although the complexity of the T−S diagram also reflects water mass modification due to air-sea interactions. The T−S diagram also shows that there is almost no overlap between early-winter distributions and summer distributions. Because the source of seawater with a salinity of ~32 and a relatively warm SST was almost certainly the Pacific Ocean, it is reasonable to conclude that water from the Pacific Ocean is cooled and freshened by mixing with local water masses and air-sea interactions during its flow northward. In Figure 6, the region of T−S space associated with the MIZ is outlined by red dashed lines. It is apparent from Figure 6 that most changes of SST in the MIZ occurred in the SSS range 31−32. Those waters were located far from the Bering Strait (Figure 1a); water with a SST greater than ~2.5°C was present only outside the MIZ. These observations support our conclusions about the water masses that enter the WAO from the Pacific Ocean. Based on observations made during MR18-05C, Kodaira et al. (2020) have reported that

horizontal advection of warm Pacific water occurs in the Chukchi Sea. The fact that changes of SST were dominant as a cause of pCO_2 changes in the MIZ is consistent with our conclusion that changes of SST accounted for most of the changes of pCO_2 in the MIZ (section 5.2).

The T−S diagram also confirmed that the ranges of SST and SSS were smaller in the early winter than in the summer, although the areas where the observations were made were not identical (Figures 1a and b). This change in the ranges of T and S is consistent with enlargement of the T−S space during the season free of sea ice (Woodgate et al., 2005) due to mixing of water from the Pacific Ocean with local water derived from melting of sea ice, especially in the Polar Mixed Layer (PML) that occupies the upper 30 m of the water column (Bates, 2006). In addition, strong winds ($>$ 10 m s^{-1}) that are observed occasionally cause local vertical mixing and promote an upward flux of nutrients from subsurface layers (Nishino et al., 2015). Inoue et al. (2021), for example, have reported that strong winds during 20–21 November 2018 mixed the entire water column from the surface to the bottom in the MIZ. Under such conditions, there is an upward flux of nutrients and homogenizing of carbonate system properties. However, we did not detect the changes of carbonate system properties that would have been expected based on conditions during those days (see Figures 2a, 3a, and 3b). The reason why no change was detected is currently unknown, but frequent prior mixing of the water column may have minimized vertical gradients of carbonate system properties and hence led to a weak signal on the observation days. Despite this result, an upward flux of nutrients and associated stimulation of photosynthesis could impact the spatial variations of the pCO_2, especially in summer. We use the TA−TCO_2 plots in Figure 7 to discuss this point further.

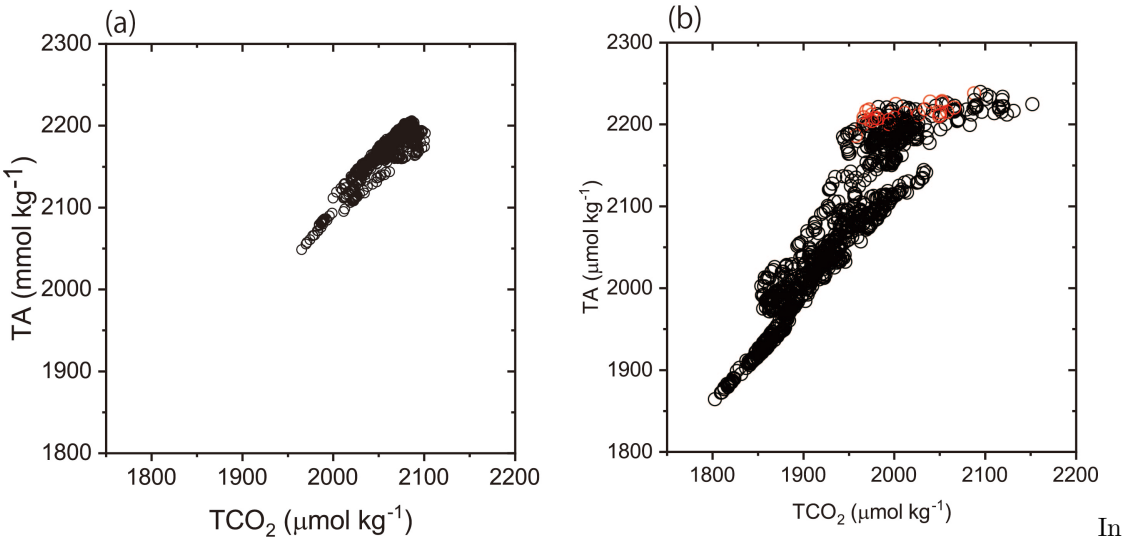

In contrast to the T−S diagram, the TA−TCO_2 plot (Figure 7a) for early winter showed a rather simple linear relationship and a positive correlation (r^2 =

0.873, $n = 872$) that implied a conservative change of properties. The slope of the regression line (1.04 ± 0.03) was nearly equal to 1.0. An enlarged version of Figure 7a (Figure S4) showed that some changes of TCO_2 were conservative, i.e., the slopes equaled ~1.0. Expected multiple slopes suggested that more than one water mass was involved in the conservative changes. Because increases of TCO_2 and TA have positive and negative effects on pCO_2, respectively (Eqs. S3 and S4), conservative changes of TCO_2 and TA would have had less of an effect on pCO_2 than changes of either parameter by itself. Because there was a negative correlation between the changes of pCO_2 due to changes of TCO_2 and TA (section 5.1), the effects of these changes on pCO_2 were suppressed compared to the effects that would have been observed, for example, if the TCO_2 had changed due to photosynthesis at a constant TA.

The conservative changes of TCO_2 and TA were distinct not only in the early winter but also in the summer (Figure 7b). The changes in the center of the TA–TCO_2 plot in summer were similar to those in winter (slope = ~1.2 in the center of Figure 7b) but the changes during summer were dissimilar at high TAs (slopes = ~0.3) to those in the early winter, and the ranges of TA and TCO_2 were larger in the summer than in the early winter. The fact that shipboard observations were made over a wider area in summer (Figures 1a and b) was probably one of the reasons for the seasonal difference. Nevertheless, it is possible that biological processes also affected the distributions of TCO_2 and TA. To test this hypothesis, we superimposed the percent saturation of dissolved oxygen (DO) on the TA−TCO_2 plots (Figure 7b). We adopted a percent saturation of 110% or more as a signal of biological production (Millero, 2006). DO supersaturations that exceeded 110% appeared at TCO_2 concentrations of 1950–2050 mol kg^{-1} at an almost constant TA of 2220 ± 10 mol kg^{-1} in the summer but not in the early winter. This result indicates that influences of biological production on the pCO_2 variations were small in both seasons, although we may have underestimated biological production because of the difference of air-sea equilibrium time between DO and CO_2. The former is about a few weeks, but the latter is over half a year.

The ratio of TA to TCO_2 (TA/TCO_2) was calculated to be 1.05 ± 0.01 for the early winter, and 1.09 ± 0.03 and 1.04 ± 0.00 for the smaller and larger slopes in the summer, respectively, despite the fact that there are many unknown water masses in the WAO. It is unclear why the ratios were close to 1.0, but it has been reported that the ratio of TCO_2 to TA in sea ice is close to 1.0 (Raysgaard et al., 2007) and that the ratio in seawater in the Bering Sea shelf, which is the source region of water masses that flow northward through the Bering Strait, is close to 1.0 because of blooms of the coccolithophorid *Emiliania huxleyi* (Murata, 2006).

We have shown that water mixing and the associated conservative changes of TCO_2 and TA have important effects on the spatial variations of surface seawater pCO_2 in both the early winter and summer. We now discuss the impacts of water mixing on the pCO_2 variations in terms of freshwater discharge, which also impacts the carbonate system in the Arctic Ocean.

In the MIZ, the end-members of TCO_2 and TA at SSS = 0 (TCO_2_0 and TA_0 in Eqs. S6 and S7) were estimated to be 15 mol kg^{-1} and 483 mol kg^{-1}, respectively (Figure S6). These values are close to those reported as end-members of sea ice meltwater (Yamamoto-Kawai et al., 2005; Ouyang et al., 2020) and support the assumption that the freshwater in the MIZ is associated exclusively with meltwater from sea ice. In fact, Yamamoto-Kawai et al. (2009) have pointed out that there is not a significant contribution of river water throughout the Canada Basin. The calculated TCO_2_0 and TA_0 for the whole study area were 1028 mol kg^{-1} and 906 mol kg^{-1} (Figure S5), respectively. The TA_0 was close to the value (~1000 mol kg^{-1}) reported for Arctic rivers (Anderson et al., 1983; Olsson and Anderson, 1997; Cooper et al., 2008). In addition, Yamamoto-Kawai et al. (2005) have calculated the end-member value of TA to be 831 ± 100 mol kg^{-1} for a mixture of meteoric water and saline deficit of Pacific water after correction for the effect of meltwater from sea ice. The higher values of each end-member suggest that the influence of freshwater is associated with sources other than meltwater from sea ice. The implication is that the dominant contribution of meltwater from sea ice to freshwater is confined to the MIZ.

6.2. CO_2 Sink Capacity

The air-sea fluxes of CO_2 were estimated to be −7.5 ± 1.6 mmol m^{-2} d^{-1} and −8.0 ± 1.7 mmol m^{-2} d^{-1} in the early winter and the summer, respectively. The area that was sampled in the present study generally corresponded to the Chukchi Sea. The CO_2 fluxes obtained in the present study could thus be compared with those for the Chukchi Sea estimated in previous studies. Murata and Takizawa (2003) have estimated CO_2 fluxes on a monthly timescale in shelf waters during two summer seasons. Their estimated fluxes were −7.9 ± 3.4 mmol m^{-2} d^{-1} and −11.3 ± 4.5 mmol m^{-2} d^{-1} in the summers (September) of 1999 and 2000, respectively. The CO_2 fluxes obtained in this study (−7.7 ± 1.9 mmol m^{-2} d^{-1}) were comparable to those values, although their calculation included the Beaufort Sea, and their transfer velocity differed from ours. Bates et al. (2006) have reported a transfer velocity of 61 ± 19 mmol m^{-2} d^{-1} in September, which is substantially different from the summertime value obtained in this study (−8.0 ± 1.7 mmol m^{-2} d^{-1}), even if the uncertainties are considered. The large difference possibly comes from the fact that the CO_2 fluxes calculated by Bates et al. (2006) were based on very low surface seawater pCO_2 values (100−160 atm). Because the low pCO_2 was calculated from discrete measurements of TCO_2 and TA at water-sampling stations, it is possible that they detected low values by chance during their observations, the number of which were relatively small compared to the number of samples collected via underway sampling. As a result, low and probably unrepresentative values may have had a large influence on the average calculated from the relatively low number of samples. The fact that we estimated a similarly low pCO_2 of ~183 atm in an area of high spatial variability of pCO_2 during the summer in this study (Figure 2d) supports this inference. In addition, recent studies (Chen et al., 2015; Sulpis et al., 2020) have discussed the errors of calculated properties

of the CO_2 system caused by applying often-used equilibrium constants to cold water. This concern may also be related to the large differences between the results of the present study and of Bates et al. (2006). Gao et al. (2012) have conducted underway pCO_2 observations in the Chukchi Sea in August and have reported CO_2 fluxes of -17.0 and -8.0 mmol m^{-2} d^{-1} in shelf and slope waters, respectively, which are comparable to the values obtained in the present study. Hauri et al. (2013) have computed monthly averaged air-sea fluxes of CO_2 from September to November in 2011. They have shown that the capacity of the CO_2 sink in the Chukchi Sea is not as strong as previously thought. They have pointed out that strong winds often mix up subsurface CO_2-rich waters into the surface layers. This upmixing reduces the CO_2 uptake or may even lead to outgassing of CO_2 (7.1 ± 7.8 mmol m^{-2} d^{-1}). We also observed CO_2 outgassing of a comparable magnitude, although the frequency of occurrence was low in our study (Figures 4b and d). Evans et al. (2015) have calculated monthly air-sea CO_2 fluxes within 0.2° latitude × 0.5° longitude pixels from ~600,000 pCO_2 measurements. They also examined the influence of sea ice cover on the CO_2 fluxes by comparing the values between pixels with and without sea ice. In September, the CO_2 fluxes were estimated to be -10.5 and -10.6 mmol m^{-2} d^{-1} for pixels with and without sea ice, respectively. These fluxes are close to the value we estimated during summer in the present study. In contrast, the CO_2 fluxes during early winter (November) were very different in the present study (-7.5 ± 1.6 mmol m^{-2} d^{-1}) and the study by Evans et al. (2015) (0.5 mmol m^{-2} d^{-1} [with sea ice] and 0.0 mmol m^{-2} d^{-1} [without sea ice]). They used basically the same data reported by Hauri et al. (2013), although additional data were combined for gridding purposes. The pattern of the monthly climatology of the CO_2 fluxes in November reported by Evans et al. (2015) (see Figure 7 in their study) shows sources and sinks of CO_2 in the southern and northern parts of shelf waters, respectively, that are similar to the distributions of the CO_2 fluxes in the present study (Figure S3b). Sparce observations combined with high spatial and temporal variability of surface seawater pCO_2 values probably caused the large differences of estimated CO_2 fluxes.

As discussed in section 4.3, there were two peaks in the histograms of the CO_2 fluxes in both the early winter and the summer (Figures 4b and d). The individual peaks correspond to the CO_2 fluxes in shelf or slope waters (Figures S3b and d). The implication is that the CO_2 sink capacity in the study area differed spatially.

7. Conclusions

We evaluated the CO_2 sink capacity of the WAO in early winter (November 2018), when few pCO_2 observations have been made because of the presence of sea ice. We found that the area acted as a sink for atmospheric CO_2 in early winter. The sink capacities were comparable in the early winter and summer. This result differed from results based on observations in previous studies, which showed that the sink capacity was weak in early winter compared with the sink capacity in summer (Hauri et al., 2013; Evans et al., 2015). In contrast, mapping

of the CO_2 fluxes for November in the present study revealed fluxes comparable to those previously reported for August and September (Yasunaka et al, 2016; 2018). Sparseness of the pCO_2 data seems to have caused these differences.

In most previous studies, biological processes and cooling have been regarded as the dominant factors that control the surface seawater pCO_2 in shelf waters of the Chukchi Sea (e.g., Kaltin & Anderson, 2006). As discussed in section 6.1, in the early winter, the relationship between TA and TCO_2 appeared to reflect conservative mixing. The slope of the relationship between TCO_2 and TA (~1.0) was consistent with simple mixing of water masses. Even during the season of high primary production (summer), the changes of TCO_2 and TA appeared to be conservative. The explanation for this conservative behavior may be that active biological production occurs during earlier seasons and/or in upstream waters (e.g., Bering Sea). We would like to emphasize that the conservative changes of TA and TCO_2 during mixing of water masses has important implications for the spatial variations of surface seawater pCO_2.

Although spatiotemporal variations of TCO_2 have been frequently discussed in terms of biological processes (Murata & Takizawa, 2003, Bates et al., 2009), TA has not been considered as often as TCO_2 in studies of oceanic CO_2 variability in the Arctic Ocean. Recently, Woosley and Millero (2020) have pointed out the importance of TA imported particularly by river water for the uptake of anthropogenic CO_2. We would like to emphasize the importance of TA in controlling air-sea exchanges of CO_2 in the WAO.

Our results may be a special case because they are based on data collected under anomalously warm conditions. However, we infer that such conditions may occur more frequently in the near future because of global warming. We therefore expect that our data will be especially helpful for future assessments of the carbon cycle.

Acknowledgments, Samples, and Data

We are grateful to the captains, crews, and marine technicians (Marine Works) of the R/V *Mirai* during the MR17-05C and MR18-05C cruises for operating and maintaining the underway measuring system for pCO_2, TCO_2, SST, and SSS. Funding for this research was provided by the Ministry of Education, Culture, Sports, Science and Technology of Japan (MEXT) through the Arctic Challenge for Sustainability (ArCS II) Project. The data used in this paper are available at the JAMSTEC web page (http://www.jamstec.go.jp/e/).

References

Anderson, L., Dryssen, D., Jones, E. & Lowing, M. (1983). Inputs and outputs of salt, fresh water, alkalinity, and silica in the Arctic Ocean. *Deep-Sea Research, Part A, 30*, 87–94.

Bakker, D. C. E., Pfeil, B., Smith, K., Hankin, S., Olsen, A., Alin, S. R., et al. (2014). An update to the Surface Ocean CO_2 Atlas (SOCAT version 2). *Earth System Science Data, 6*, 3269–3340. doi.org/10.5194/essd-6-69-2014

Bakker, D. C. E., Pfeil, B., Landa, C. S., Metzl, N., O'Brien, K. M., Olsen, A. et al. (2016). A multi-decade record of high-quality fCO_2 data in version 3 of the Surface Ocean CO_2 Atlas (SOCAT). *Earth System Science Data, 8*, 383–413. doi.org/10.5194/essd-8-383-2016

Bates, N. R. (2006). Air-sea CO_2 fluxes and continental shelf pump of carbon in the Chukchi Sea adjacent to the Arctic Ocean. *Journal of Geophysical Research, 111*, C10013, doi:10.10129/2005JC003083

Bates, N. R., Moran, S. B., Hansell, D. A., & Mathis, J. T. (2006). An increasing CO_2 sink in the Arctic Ocea due to sea-ice loss. *Geophysical Research Letters, 33*, L23609. doi:10291/2006GL027028

Bates, N. R., Mathis, J. T., & Cooper, L. W. (2009). Ocean acidification and biologically induced seasonality of carbonate mineral saturation states in the western Arctic Ocean. *Journal of Geophysical Research, 114*, C11007, doi:10.1029/2008JC004862

Burgers, T. M., Miller, L. A., Thomas, H., Else, B. G. T., Gosselin, M., & Papakyriakou, T. (2017). Surface water pCO_2 variations and sea-air CO_2 fluxes during summer in the Eastern Canadian Arctic. *Journal of Geophysical Research: Oceans, 122*, 9663−9678. https://doi.org/10.1002/2017JC013250

Cai, W.-J., Bates, N. R., Guo, L., Anderson, L. G., Mathis, J. T., Wanninkhof, R. et al. (2014). Carbon Fluxes Across Boundaries in the Pacific Arctic Region in a Changing Environment. In J. M. Grebmeier, W. Maslowski (Eds.) *The Pacific Arctic Region: Ecosystem Status and Trends in a Rapidly Changing Environment*, doi:10.1007/978-94-017-8863-2_8

Chen, B., Cai, W.-J., & Chen, L. (2015). The marine carbonate system of the Arctic Ocean: Assessment of internal consistency and sampling considerations, summer 2010. *Marine Chemistry, 176*, 174–188.

Coachman, L. K., Aagaard, K., & Tripp, R. B. (1975). *Bering Strait: The Regional Physical Oceanography,* Univ. of Wash. Press, Seattle, 172 pp.

Cooper, L. W., McClelland, J. W., Holmes, R. M., Raymond, P. A., Gibson, J. J., Guay, C. K., & Peterson, B. J. (2008). Flow-weighted values of runoff tracers (^{18}O, DOC, Ba, alkalinity) from the sex largest Arctic rivers. *Geophysical Research Letters, 35*, L18606. doi:10.1029/2008GL035007

Evans, W., Mathis, J. T., Cross, J. N., Bates, N. R., Frey, K. E., Else, B. G. T., et al. (2015). Sea-air CO_2 exchange in the western Arctic coastal ocean. *Global Biogeochemical Cycles, 29*, 1190–1209. doi:10.1002/2015GB005153

Friis, K., Krtzinger, K., & Wallace, D. W. R. (2003). The salinity normalization of marine inorganic carbon chemistry data. *Geophysical Research Letters, 30*(2), doi:10.1029/2002GL015898

Friedlingstein, P., O'Sullivant, M., Jones, M. W., Andrew, R. M., Hauck, J., Olsen, A., et al. (2020). Global carbon budget. *Earth System Science Data, 12*,

3269–3340. doi.org/10.5194/essd-12-3269-2020

Gao, Z., Chen, L., Sun, H., Chen, B., & Cai, W. J. (2012). Distributions and air–sea fluxes of carbon dioxide in the Western Arctic Ocean. *Deep-Sea Research II, 81–84*, 46–52.

Gong, D., & Pickart, R. S. (2015). Summertime circulation in the eastern Chukchi Sea. *Deep-Sea Research, Part II*, 118, 18–31. https://doi.org/10.1016/j.dsr2.2015.02.006

Hauri, C., Winsor, P., Juranek, L. W., McDonnell, A. M. P., Takahashi, T., & Mathis, J. T. (2013). Wind-driven mixing causes a reduction in the strength of the continental shelf carbon pump in the Chukchi Sea. *Geophysical Research Letters, 40*, 5932–5936. doi: 10.1002/2013GL058267

Iida, Y., Kojima, A., Takatani, Y., Nakano, T., Sugimoto, H., Midorikawa, T., & Ishii, M. (2015). Trends in pCO_2 and sea-air CO_2 flux over the global open oceans for the last two decades. *Journal of Oceanography, 71*, 637–661. doi:10.1007/s10872-015-0306-4

Inoue, J. (2021). Review of forecast skills for weather and sea ice in supporting Arctic navigation. *Polar Science, 27*, https://doi.org/10.1016/j.polar.2020.100523

Inoue, J., Tobo, Y., Taketani, F., & Sato K. (2021). Ocean supply of ice-nucleating particles and its effect on ice cloud formation: A case study in the Arctic Ocean during a cold air outbreak in early winter. *Geophysical Research Letters, 48*, e2021GL094646. https://doi.org/10.1029/2021GL094646

IOCCP (2007). Surface ocean CO_2 variability and vulnerabilities workshop. In I*OCCP Report 6.* pp.11−14. Retrieved from http://www.ioccp.org/index.php/documents/meeting-reports

Kaltin, S. & Anderson, L. G. (2005). Uptake of atmospheric carbon dioxide in Arctic shelf seas: evaluation of the relative importance of processes that influence pCO_2 in water transported over the Bering-Chukchi Sea shelf. *Marine Chemistry, 94*, 67−79.

Kodaira, T, Waseda, T., Nose, T., & Inoue, J. (2020). Record high Pacific Arctic seawater temperatures and delayed sea ice advance in response to episodic atmospheric blocking. *Scientific Reports, 10*, 20830. https://www.nature.com/articles/s41598-020-77488-y

Landschützer, P., Gruber, N., Bakker, D. C. E., & Schuster, U. (2014). Recent variability of the global ocean carbon sink. *Global Biogeochemical Cycles, 28*, 927−949. doi:10.1002/2014GB004853

Large, W. G. & Pond, S. (1981). Open ocean momentum flux measurements in moderate to strong winds. *Journal of Physical Oceanography, 11*(3), 324−336.

Lauvset, S. K., Chierici, M., Counillon, F., Omar, A., Nondal, G., Johannessen, T., & Olsen, A. (2013), Annual and seasonal fCO_2 and air–sea CO_2 fluxes in the Barents Sea. *Journal of Marine Systems, 113–114*, 62–74.

Lewis, E., & Wallace, D. W. R. (1998). Program developed for CO_2 System Calculations. ORNL/CDIAC-105. Carbon Dioxide Information Analysis Center, Oak Ridge National Laboratory, U.S. Department of Energy, Oak Ridge, Tennessee.

Lueker, T. J., Dickson, A. G., & Keeling, C. D. (2000). Ocean pCO_2 calculated from dissolved inorganic carbon, alkalinity, and equations for K_1 and K_2: Validation based on laboratory measurements of CO_2 in gas and seawater at equilibrium. *Marine Chemistry, 70*(1–3), 105–119.

Mehrbach, C., Culberson, C. H., Hawley, J. E., & Pytkowicz, R. M. (1973). Measurement of the apparent dissociation constants of carbonic acid in seawater at atmospheric pressure. *Limnology and Oceanography 18*, 897-907.

Millero, F. J. (2006). *Chemical Oceanography*, *Third edition*, CRC Press.

Murata, A., & Takizawa, T. (2003). Summertime CO_2 sinks in shelf and slope waters of the western Arctic Ocean. *Continental Shelf Research, 23*, 753–776.

Murata, A. (2006). Increased surface seawater pCO_2 in the eastern Bering Sea shelf: An effect of blooms of coccolithophorid *Emiliania huxleyi*? *Global Biogeochemical Cycles, 20*, GB4006, doi:10.1029/2005GB002615

Nakaoka, S., Aoki, S., Nakazawa, T., Hashida, G., Morimoto, S., Yamanouchi, T., & Yoshikawa-Inoue, H. (2006). Temporal and spatial variations of oceanic pCO_2 and air-sea CO_2 flux in the Greenland Sea and the Barents Sea. *Tellus 58B*, 148–161.

Nishino, S., Kawaguchi, Y., Inoue, J., Hirawake, T., Fujiwara, A., Futsuki, R., et al., (2015). Nutrient supply and biological response to wind-induced mixing, internal motion, internal waves, and currents in the northern Chukchi Sea. *Journal of Geophysical Research, Oceans, 120*, 1975–1992, doi:10.1002/2014JC010407

Olsson, K., & Anderson, L. (1997). Input and biogeochemical transformation of dissolved carbon in the Siberian shlf seas. *Continental Shelf Research, 17*, 819–833.

Omar, A. M., Johannessen, T., Olsen, A., Kaltin, S., & Rey, F. (2007). Seasonal and interannual variability of the air–sea CO_2 flux in the Atlantic sector of the Barents Sea. *Marine Chemistry, 104*, 203–213.

Ouyan, Z., Qi, Z., Chen, L., Takahashi, T., Zhong, W., Degrandpre, M. D., et al. (2020). Sea-ice loss amplifies summertime decadal CO_2 increase in the western Arctic Ocean. *Nature Climate Change*, doi.org/10.1038/s41558-020-0784-2.

Pfeil, B., Olsen, A., Bakker, D. C. E., Hankin, S., Koyuki, H., Kozyr, A., et al. (2013). A uniform quality controlled Surface Ocean CO_2 Atlas (SOCAT). *Earth System Science Data, 5*, 125—143. doi:10.5194/essd-5-125-2013.

Raysgaard, S., Glud, R. N., Sejr, M. K., Bendtsen, J. & Christensen, P. B. (2007). Inorganic carbon transport during sea ice growth and decay:

a carbon pump in polar sea. *Journal Geophysical Research, 112*, C03016. doi:10.1029/2006JC003572.

Rödenbeck, C., Keeling, R. F., Bakker, D. C. E., Metzl, N., Olsen, A., Sabine, C. et al. (2013). Global surface-ocean pCO_2 and sea-air CO_2 flux variability from an observation-driven ocean mixed layer scheme. *Ocean Science, 9*, 193−216. doi:10.5194/os-9-193-2013.

Sabine, C. L., Hankin, S., Koyuk, H., Bakker, D. C. E., Pfiel, B., Olsen, A., et al. (2013). Surface Ocean CO_2 Atlas (SOCAT) gridded data products. *Earth System Science Data, 5*, 145−153. doi:10.5194/essd-5-145-2013.

Sarmiento J. L. & Gruber, N. (2006). Carbon cycle. In *Ocean Biogeochemical Dynamic*, pp 318–358. Princeton University Press.

Sulpis, O., Lauvset, S. K., & Hagens M. (2020). Current estimates of K_1* and K_2* appear inconsistent with measured CO_2 system parameters in cold oceanic regions. *Ocean Science, 16*, 847–862. doi.org/10.5194/os-16-847-2020

Takahashi, T., Sutherland, S. C., Sweeney, C., Poisson, A., Metzl, A., Tilbrook, B., et al. (2002). Global sea−air flux of CO_2 based on climatological surface ocean pCO_2, and seasonal biological and temperature effects. *Deep-Sea Research II, 49*, 1601−1622.

Takahashi, T., Suterhland, S. C., Wanninkhof, R., Sweeney, C., Feely, R. A., Chipman, D. W., et al. (2009). Climatological mean and decadal change in surface ocean pCO_2 and net sea−air CO_2 flux over the global oceans. *Deep-Sea Research II, 56*, 554−577.

Uppstrom, L. R. (1974). The boron/chlorinity ratio of deep-sea water from the Pacific Ocean. *Deep-Sea Research 21*, 161-162.

Wanninkhof, R. (2014). Relationship between wind speed and gas exchange over the ocean revisited. *Limnology and Oceanography: Methods 12*, 351–362.

Weiss, R. F. (1974). Carbon dioxide in water and seawater: the solubility of a non-ideal gas. *Marine Chemistry, 2*, 203–215.

Woodgate, R. A., Agaard, K., & Weingartner, T. J. (2005). A year in the physical oceanography of the Chukchi Sea: Moored measurements from autumn 1990−1991. *Deep-Sea Research II, 52*, 3116−3149.

Woosley, R. J., Millero, F. J., & Takahashi, T. (2017). Internal consistency of the inorganic carbon system in the Arctic Ocean. *Limnology and Oceanography: Method, 15*, 887–896. https://doi:10.1002/lom3.10208.

Woosley, R. J. & Millero, F. J. (2020). Freshening of the western Arctic negates anthropogenic carbon uptake potential. *Limnology and Oceanography, 65*, 1834–1846.

Yamamoto-Kawai, M., Tanaka, N., & Pivovarov, S. (2005). Freshwater and brine behaviors in the Arctic Ocean deduced from historical data of ^{18}O and

alkalinity (1929−2002 A.D.). *Journal of Geophysical Research, 118*, C10003, doi:10.1029/2004JC002793.

Yamamoto-Kawai, M., McLaughlin F. A., Carmack, E. C., Nishino, S., Shimada, K. & Kurita, N. (2009). Surface freshening of the Canada Basin, 2003−2007: River runoff versus sea ice meltwater. *Journal of Geophysical Research, 114*, C00A05, doi:10.1029/2008JC005000.

Yasunaka, S., Murata, A., Watanabe, E., Chierici, M., Fransson, A., van Heuvan, S., et al. (2016). Mapping of the air-sea CO_2 flux in the Arctic Ocean and its adjacent seas: Basin-wide distribution and seasonal and interannual variability. *Polar Science, 10*, 323−334.

Yasunaka, S., Siswanto, E., Olsen, A., Hoppema, M., Watanabe, E., Fransson, A., et al., (2018). Arctic Ocean CO_2 uptake: an improved multiyear estimate of the air–sea CO_2 flux incorporating chlorophyll a concentrations. *Biogeosciences, 15*, 1643–1661. doi.org/10.5194/bg-15-1643-2018.